OTKA (NKFIH) Consortium Grant – Report

Development of novel silicon carbide nanomarkers and more effective glutamate and GABA uncaging materials for the measurement of neuronal network activity and dendritic integration with three-dimensional real-time two-photon microscopy

Consortium Leader:	**Dr. Balázs Rózsa**
Hosting Institution:	**Institute of Experimental Medicine, Hungarian Academy of Sciences, IEM HAS**
Principal Investigator:	**Dr. Adam Gali (consortium partner)**
Hosting Institution:	**Institute for Solid State Physics and Optics, Wigner Research Centre for Physics (Wigner RCP), Hungarian Academy of Sciences (HAS)**
Consortium Partners:	**Dr. Pál Maák (Department of Atomic Physics, BME), Prof. Perlné dr. Ibolya Molnár (ELTE)**
Project duration:	**2012.09.01-2016.08.31. (2017.12.31)**

Specific goals of the project

1. Three dimensional two-photon uncaging of glutamate and GABA in order to change local and global membrane potential

We have developed ca. 20 novel caged-neurotransmitter (e.g. glutamate **1**–**4**; see **Scheme 1**; GABA),[2–4] which are under testing by 2-photon microscope.[1] Some of them performs relatively well in neurophotonical experiments. We have published several high impact papers using the novel caged compounds. Our novel DNI glutamate is ~5-7-fold more effective in photochemical release than the world "best" caged glutamate, MNI-glutamate, comfirmed by analitical tools [5] and in silico calculations.[6]

1.1. Synthesis and development and characterization of novel caged glutamate neurotransmitters for three dimensional two-photon uncaging

We have synthesized the trifluoro acetate (TFA) form of MNI-Glu, as MNI-Glu•TFA (**1**; 4-methoxy-5-nitro-indolyle-γ-glutamate trifluoro-acetate) and its three close analogues DNI-Glu•TFA (**2**; 4-methoxy-5,7-dinitro-indolyle-γ-glutamate trifluoro-acetate), MNI-Ulg•TFA (**3**; 4-methoxy-5-nitro-indolyle-α-glutamate trifluoro-acetate) and DNI-Ulg•TFA (**4**; 4-methoxy-5,7-dinitro-indolyle-α-glutamate trifluoro-acetate) in order to compare their efficacy in two-photon uncaging experiments (**Scheme 1**). The TFA salt proved to be more stable in solid form at –20 °C, and being more resistant toward hygroscopic degradation, yet TFA does not influenced the biological investigations. Moreover, the solvation of the solid sample is more rapid.

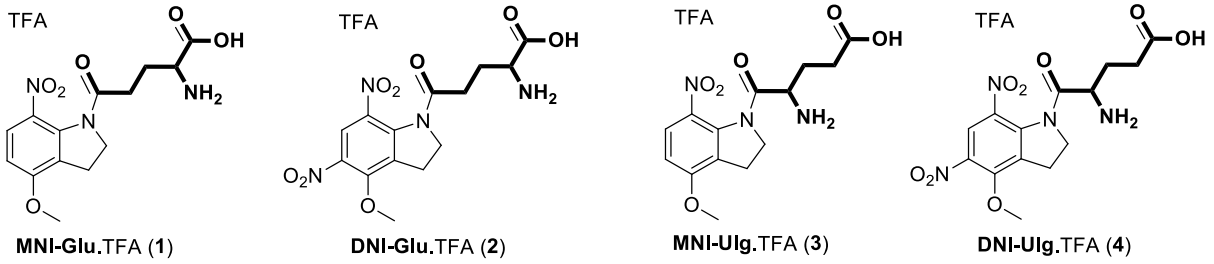

Scheme 1*. The synthetized cage-glutamate compounds*

1.1.1. Synthesis of novel cage glutamate compounds

The synthesis of MNI-Glu (**1**) was carried out according to a previously published method (**Scheme 2**), but it proved to be very inefficient, consequently some modifications of the reaction conditions were made to optimize the original low yield. The synthesis of **2**–**4** were started on the same route (**Scheme 2**), starting from the methylation of the 4-hydroxy-indole, leading to **6**, then its reduction by $NaBH_3CN$. The 4-methoxy-indoline (**7**) was acylated by differently protected glutamic acids [Boc-Glu(OtBu)-OH - **8** and Boc-Glu-OtBu – **9**], resulting the so called Glu- (**10**) and Ulg-derivatives (**11**), respectively. However, selective of mononitration and dinitration requires distinct procedures. The original, $AgNO_3$/AcCl reagent combination (Route A) was found to be the best choice for the selective mononitration at position 7 under dark condition. Here, the deprotection of **12** and **13** were carried out in a separate step by TFA, yielding MNI-Glu (**1**) and MNI-Ulg (**3**), respectively.

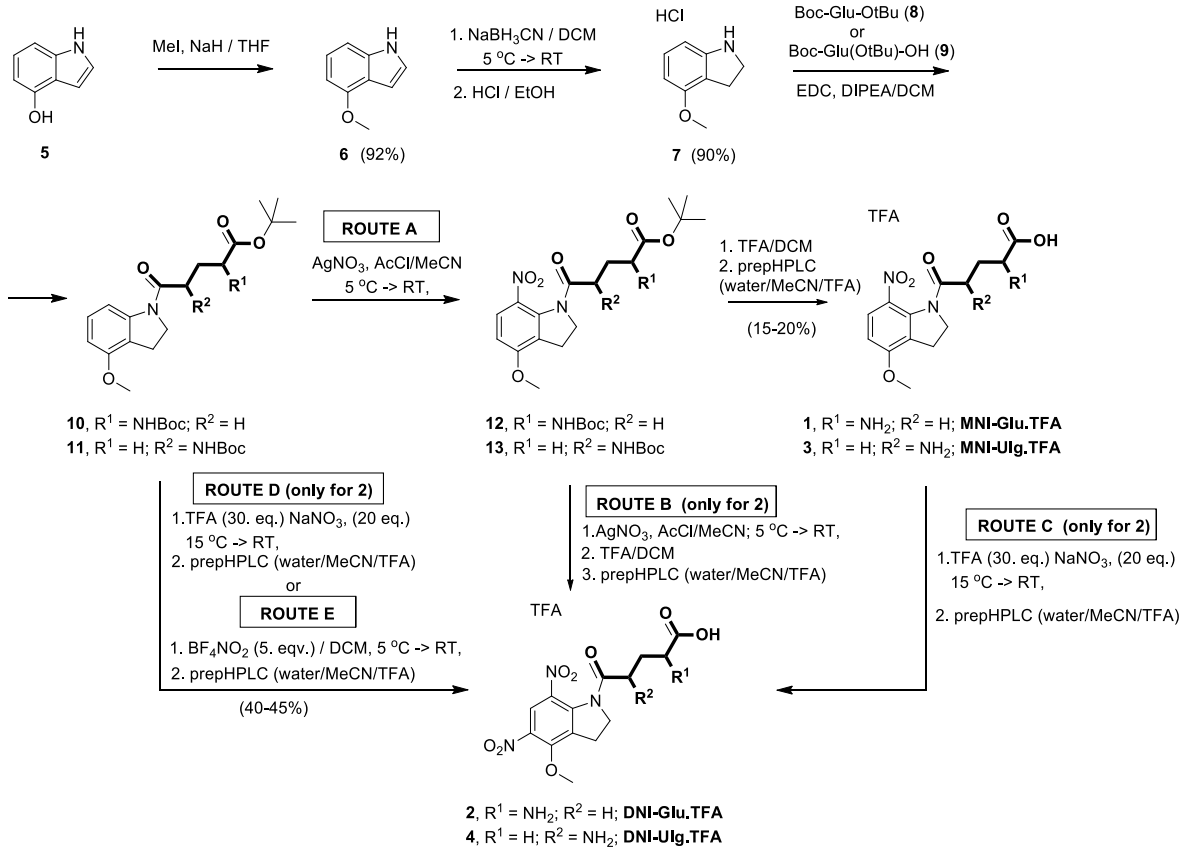

Scheme 2. *The synthetic scheme of the trifluoroacetate salts of MNI-Glu (**1**), DNI-Glu (**2**), MNI-Ulg (**3**) and DNI-Ulg (**4**), including five **Routes A–E**. For details see [6]*

A selective and productive dinitration procedure, however, required more development (Route B–E), carried out only for the synthesis DNI-Glu (**2**, **Scheme 2**). Further nitration of the protected mononitro compound **12**, by using $AgNO_3$/AcCl reagent, resulted the desired product in low yield. This may be due to the moderate activity of the reagent (Route B). Stronger nitration condition, the $NaNO_3$ in TFA solvent, was elaborated on compound **1** (Route C), which resulted significant amount of degraded side-product during the work-up. The same nitration condition was also tried on compound 10 (Route D), where the desired product was formed in one step, but in a moderate yield.
Moreover, the large excess of TFA caused difficulties during work-up. Finally, the one-pot dinitration (Route E) of **10** later **11** by 3 equivalents of $NO_2 \cdot BF_4$ in dry DCM, at low temperature (0–5 °C), was also carried out.

1.2. Measurement and calculation of two-photon absorption (IEM HAS, BME)

We computed the two-photon absorption (TPA) cross-section (σ) of the two, most potent uncaging compounds, MNI-Glu (**1**) and DNI-Glu (**2**), using DALTON 2.0 program in gas phase at B3LYP/6-31G(d,p) level of theory.[6] The TP transition moment tensor components (S) were calculated and analyzed (**Table 1**). As can be seen from these data, the S_{xx} is the highest tensor component for both compounds **1** and **2**, while the contribution of the other tensor components proved to be almost negligible. It appears that a charge transfer from OMe to NO_2 along the x direction (behaves as an antenna) plays an important role in determining the net transition probability *(TP) of these molecules.*

***Table 1**. The computed two-photon transition tensor components (S) for the S_0–S_1 transition of MNI-Glu (**1**) and DNI-Glu (**2**) computed at B3LYP/6-31G(d,p) level of theory by using DALTON 2, assuming monochromatic light source with linear polarization.*

Compounds	**MNI-Glu (1)**	**DNI-Glu (2)**
S_{xx}	13.5	28.6
S_{yy}	0.3	0.4
S_{zz}	0.1	0.1
S_{xy}	–0.4	–2.9
S_{xz}	–0.7	–0.4
S_{yz}	0.2	0.1

The TPA cross section values (σ) calculated from linear transition probability (D) and the excitation energy (E) (**Table 2**), based on a method published earlier. The results show about a 4.3 time larger σ value for DNI-Glu (**2**) than that of MNI-Glu (**1**). These results predict almost 5 times larger TPA for the S_0–S_1 excitation, which influence positively, the overall photochemical process.

***Table 2**. Two-photon transition energy (E in eV), probabilities (D_f, D_g and D in a.u.) cross section values (σ in a.u. as well as in GM) for the S_0–S_1 transition of MNI-Glu (**1**) and DNI-Glu (**2**) computed at B3LYP/6-31G(d,p) level of theory by using DALTON 2, assuming monochromatic light source with linear polarization.*

Compounds	**MNI-Glu (1)**	**DNI-Glu (2)**	**Ratio**
E (eV)	3.20	3.12	–
D_f (a.u.)	65.0	282	**4.34**
D_g (a.u.)	61.4	278	**4.53**
D (a.u.)	376	1676	**4.46**
σ (a.u.)	6.94	29.4	**4.24**
σ (GM)	13.16	55.75	**4.24**

According to our experimental and computational results, we can transform our enthalpy values to kinetical information and explain the differences between MNI-Glu (**1**) and DNI-Glu (**2**), observed during the neurobiological uncaging experiments. The difference between **1** and **2** can be traced back to three branching points (labelled by the Arabic numerals I, II, and III; **Figure 1**). Initially at point I, a small percentage of the compounds (0.1% for MNI-Glu (**1**) and 3% for DNI-Glu, (**2**) respectively) hydrolyses spontaneously. The remnants (99% and 97%, respectively) undergo excitation. At point II about nine times as much DNI-Glu (90%) undergoes dissociation compared to MNI-Glu (9.9%). This data, 11% agrees well with the experimentally determined QY (8.5%). In the final stage, at point III, only 0.1% of the compound is hydrolysed. Consequently, DNI-Glu (**2**) is the most effective of the four compounds, in excellent agreement with experiments.

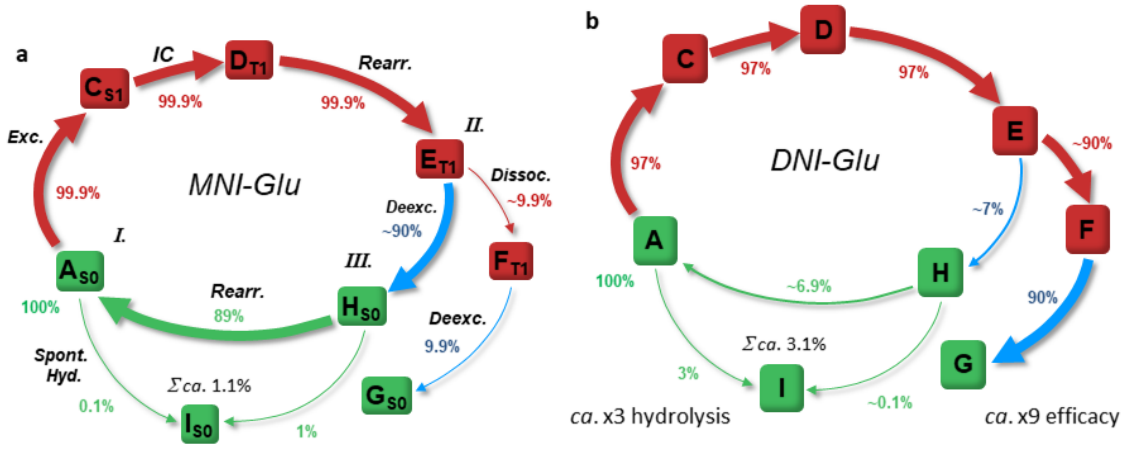

Figure 1. *(**a**, **b**): Symbolic representation of the mechanism underlying photochemical release and spontaneous hydrolysis of DNI-Glu (**2**), MNI-Glu (**1**). The thickness of these lines corresponds to the efficiency of the individual steps, based on a semiquantitative combination of theoretical and experimental results. These numerical estimates of efficiency (in %) of each step is indicated. Branching points are marked by I, II, and III. Red, green, and blue arrows indicate excitation, rearrangement, and de-excitation parts of the schemes, respectively.*

1.3 Following the stability of caged compounds by means of the analysis of amino group-containing metabolites (ELTE)

A simultaneous, simple and cost efficient identification andquantification protocol for ICGs and their decomposition products(free amino acid, uncaged species) was described, as novelty to thefield, from one solution partly as OPA/MPA derivatives, partly asspecies in their initial forms: applying tandem DAD and Fl detections.Studies on derivatization properties and spectral characteristics of variously substituted ICGs proved that without derivatization they show up with characteristic, different maxvalues, while, their OPA derivatives, independent on the SH group additive, confirmed the maxvalue at 337 nm, without exception (**Figure 2**). Uncaged species manifested the same, or approximately the same UV properties as their underivatized, caged versions. As to the stoichiometrical identities of ICGs' OPA deriva-tives, followed by HPLC–TOF-MS, they were confirmed by theirexact molecular masses. Also, the SH-additive of the reagentswas varied: composition of all derivatization product proved the[OPA/SH]/[ICG] = 1/1 molar ratios, manifesting the characteristic isoindole structure. Practical utility of this method was fully validated. This proposal (suitable at first for the simultaneousquantitation of ICGs and their hydrolysis products) served forproof of stability comparison, both of already known and/or newly introduced ICGs. In addition, this method served also as contribution to the right ICGs species selection for biologists and microscopedesigner specialists in their uncaging studies, meaning, the stimulation of neurons activity in living cells.

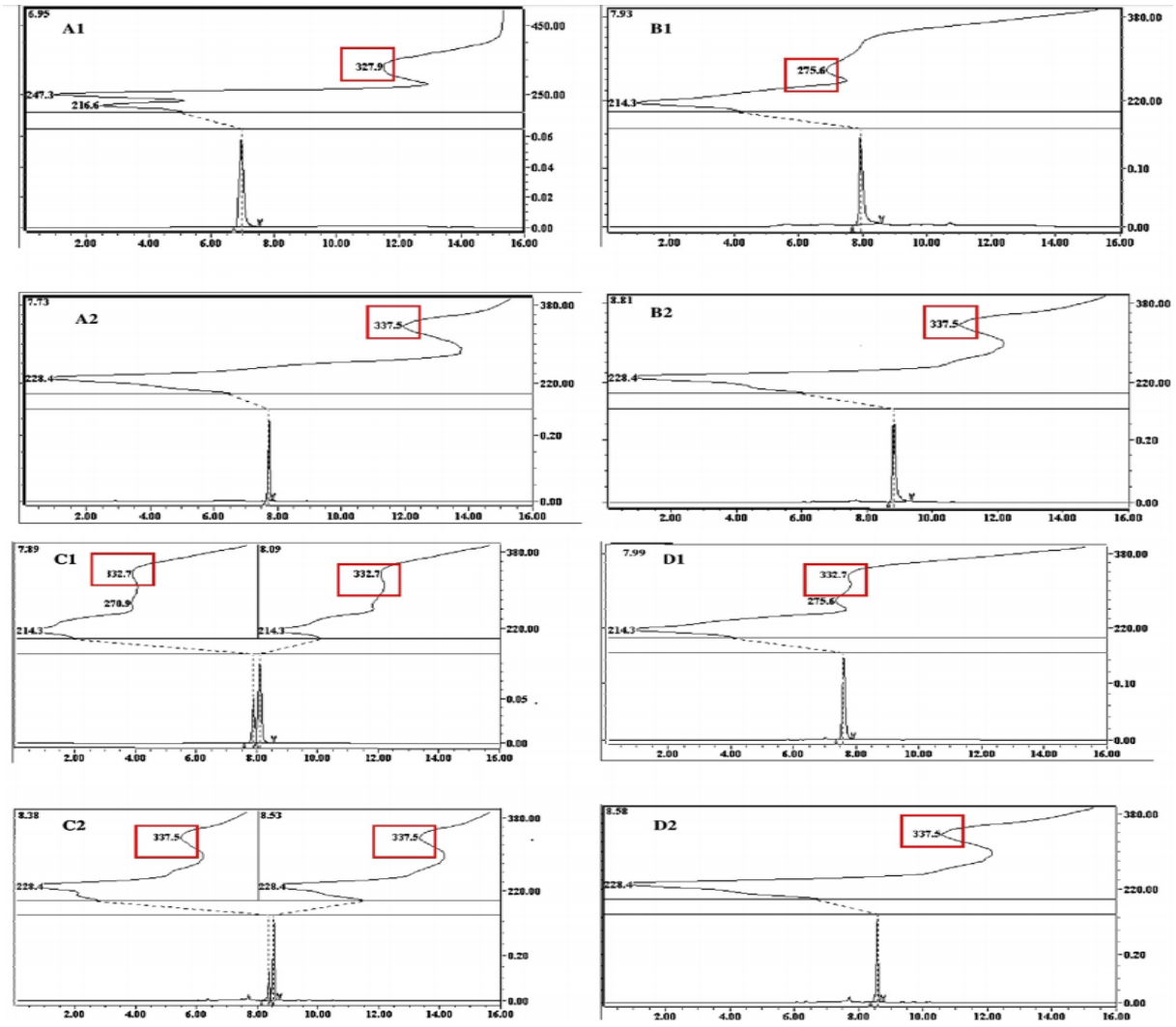

Figure 2*. UV chromatograms and DAD spectra of MNI-Glu (A1), DNI-Glu (B1), isomers of 2DMA-1PO-DNI-Glu (C1) and iDMBO-Glu (D1) and OPA–MPA derivatives of MNI-Glu (A2), DNI-Glu (B2), iDMPO-Glu (C2) and 3DMA-1Bu-DNI-Glu (D2); chromatograms were extracted at 328 nm (A1), 276 nm (B1), 333 nm (C1 and D1), and 337 nm (A2–D2), respectively.*

1.4 In vitro functional measurements and characterization of cellular toxicity using the new caged neurotransmitter

1.4.1. Technical detail

For in vivo measurement male or female C57Bl/6J wild-type mice (postnatal age 60–130 days) were used. The procedure for surgery and *in vivo* bolus loading were performed as previously described (Katona et al. 2012). Bulk loading was performed with a patch pipette using Oregon Green BAPTA-1 AM (2 mM, Invitrogen) or SiC NPs and sulforhodamine-101 (200 μM, Invitrogen) under two-photon guidance (810 nm), and a cover glass was fixed to the skull above the cranial window, along with a light-shielding cone. Cell imaging will be started 1 h after dye loading to allow for proper staining.

Three dimensional imaging was performed using the 3D acousto optical microscope (pulished in Nature Methods). This setup is able to scan a near cubic-millimeter volume (700 x 700 x 1400 μm^3) up to ~50/points/kHz temporal resolution. The setup will be able to perform chromatic analysis of the emitted luminescence as well as allows tuning of the excitation wavelength with minimum adjustment need regarding scanner and pulse compressor. The acousto-optic scanner performing 3D scanning will be reconstructed based on new acousto-optic cells that are optimized for wavelength tuning. These new devices will be developed at BME; at least two sets for different central wavelengths needed for

uncaging experiments. After achieving whole-cell mode and filling the interneurons with 60 μM OGB-1, the bath solution will be exchanged to ACSF containing 2.5 mM of caged glutamate or GABA compound. Photolysis of caged glutamate will be performed with second ultrafast pulsed laser light (690-850 nm Mai Tai HP Deep See; SpectraPhysics). Analysis of 3D measurements will be done using programs developed by the Two Photon Image Center of IEM HAS. The required modifications of the 3D microscope (new detectors and the completion of the system with the second laser pathway) have been performed by Maák Pál (BME), Gergely Katona (IEM HAS), Gergely Szalay (IEM HAS).

1.4.2. Neurobiological Results

It is known, that MNI-Glu (**1**) tends to hydrolyze spontaneously under aqueous condition, releasing the glutamate in an undesired process, causing difficulties in long-term measurements. It was reported earlier, that DNI-Glu (**2**) exhibits faster hydrolysis. In order to avoid the numerous negative effects of spontaneous hydrolysis, and therefore allow the use of caged compounds with high QY value (*e.g*. **2**), it was necessary to develop a selective method for the free glutamate elimination, which does not influence the concentration of the caged compound and has no side effects on the tissue. The use of enzymes, being selective for their substrates and effective in very low concentrations, seem to be an obvious choice. Two key processes are responsible for glutamate degradation: transamination and deamination. We chose glutamate dehydrogenase (**Scheme 3**), because its coenzyme, nicotinamide adenine dinucleotide phosphate ($NADP^+$) is not metabolized in the brain tissue.[47] To determine the required enzyme and coenzyme concentration, first we estimated the spontaneous hydrolysis rate of DNI-Glu•TFA (**2**), which was determined earlier. While, the unit activity of glutamate dehydrogenase is defined for the reverse direction (for 2-oxoglutarate to glutamate conversion), consequently the rate of the forward reaction is estimated to be more than one order of magnitude slower. It is important to note that the rate of added glutamate elimination is approximately 6 orders of magnitude smaller than the rate of glutamate uptake in acute slices; therefore, the enzymatic method does not interfere with the glutamate uptake system in small tissue volumes. At the same time, it effectively eliminates increased glutamate levels in the whole perfusion volume.

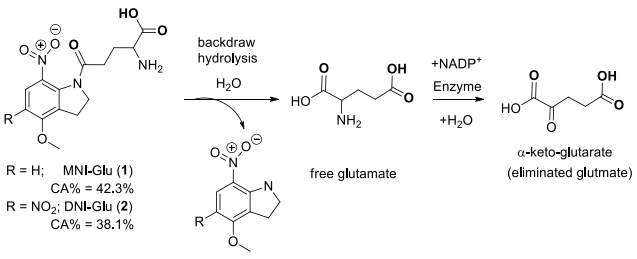

Scheme. 3*. Enzymatic reduction. The enzyme was glutamate dehydrogenase in the presence of* $NADP^+$.

Two enzyme concentrations were tried, a lower 200–520 units l^{-1} and a higher 2000-5200 units l^{-1}. This enzymatic reaction effectively decreased glutamate concentration (pink and green in **Figure 3**) compared to the control experiment (blue in **Figure 3**). The higher enzyme concentration improved the efficiency of glutamate elimination (**Figure 3**). As expected, the enzymatic reaction was sufficiently selective, the enzyme did not decrease the concentration of the caged compound [without enzyme: 2.4 ± 0.019 mM, with enzyme: 2.39 ± 0.019 mM, p = 0.66, t-test; DNI-Glu•TFA (**2**) within 136 min, [6]. However, the efficiency of the method decreased with longer measurement times. Most of the laboratories, where uncaging experiments are performed, freeze and reuse solutions of caged materials,

and therefore need efficient glutamate elimination in a longer time window. The effect of the enzyme was validated also in physiological measurements in the presence of DNI-Glu•TFA (**2**), since the amplitude of the uncaging-evoked responses did not change significantly during the experiments ($8.2\times10^{-4} \pm 4.1\times10^{-5}$ %/s, p = 0.84).

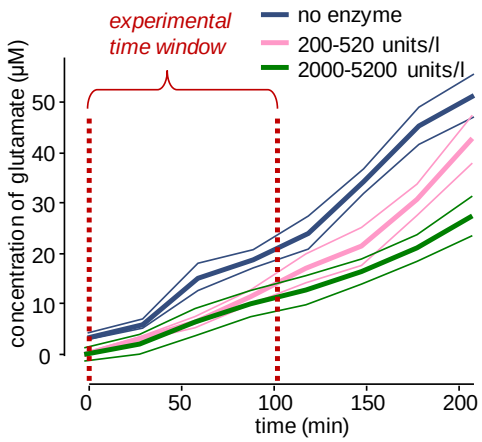

***Figure 3**. Hydrolysis curves of DNI-Glu•TFA (**2**) in 2.5 mM measured under control condition (blue), and when 200-520 units l^{-1} (pink) or 2000-5200 units/l (green) enzyme and its coenzyme (200 μM $NADP^+$) were added. Measurements were performed in ACSF buffer at pH 7.4 at 309 K. The free glutamate was determined via OPA/MPA derivatization by HPLC, based on earlier experiences.*

Next, we investigated whether electrophysiological measurements could be improved by the use of this novel enzymatic elimination method. It is known, that even a small increase in ambient glutamate level results in NMDA receptor activation and, therefore it enhances neuronal excitability,[40] increasing the rate of ongoing synaptic activity in whole-cell recorded neurons. Indeed, the frequency of spontaneous excitatory postsynaptic potentials (EPSPs) in CA1 pyramidal neurons increased, when DNI-Glu•TFA (**2**) was added to the bath perfusion (control: 1.64 ± 0.34 Hz; in the presence of DNI-Glu•TFA (**2**): 3.87 ± 0.67 Hz, n = 8, p < 0.01, *t*-test). Albeit the enzymatic method was not able to fully eliminate glutamate increase, as shown in **Figure 4**, it effectively decreased the unwanted EPSP frequency to the control value (1.71 ± 0.29 Hz; p > 0.3, n=8; **Figure 4**), indicating the physiological efficiency of the method. The increase in EPSP rate could not be the consequence of dendritic filtering or any alteration in our recording conditions, as the amplitude of EPSPs did not change throughout these experiments (control: 1.07 ± 0.16 mV; in DNI-Glu•TFA (**2**): 1.11 ± 0.28 mV, p = 0.9, *t*-test; when enzyme was added: 1.05 ± 0.21 mV, n = 3, p = 0.93, *t*-test). The use of the enzymatic elimination method allows a more precise comparison of the overall photochemical yield of MNI-Glu•TFA (**1**), DNI-Glu•TFA (**2**), since the modulatory effect of the elevated ambient glutamate concentration is eliminated.

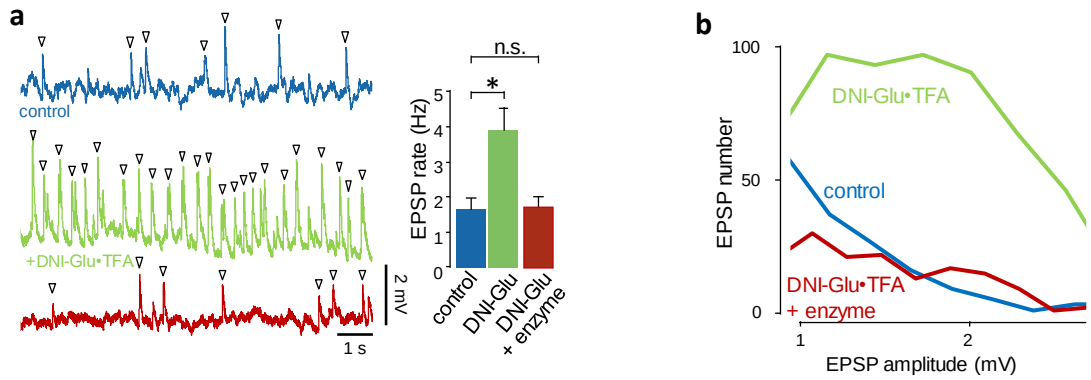

Figure 4. Enzymatic method to compensate for the spontaneous hydrolysis of caged materials. *(**a**) Spontaneous somatic EPSPs recorded from a CA1 pyramidal cell under control conditions (blue), increased EPSPs in the presence of DNI-Glu•TFA (**2**, green), and normalised EPSPs, when the enzyme and its substrate ($NADP^+$) was also added to the perfusion solution containing **2** (red). (**b**) Frequency change of spontaneous EPSPs recorded in n = 7 CA1 pyramidal neurons (mean±s.e.m.). EPSP frequency returned to its original value when the enzyme and its substrate was added (* and n.s. indicate p < 0.05 and non-significant difference, respectively). Corresponding amplitude histogram of spontaneous EPSPs.*

*1.4.3. Neurobiological comparison experiment at constant laser intensity of caged compounds **1**–**4** (Method A)*

For the comparison of the efficacy of the known MNI-Glu•TFA (**1**) as well as its modified compounds DNI-Glu•TFA (**2**), MNI-Ulg•TFA (**3**), and DNI-Ulg•TFA (**4**), were activated on the same temporally and spatially clustered patterns of inputs on hippocampal neurons. The uncaging effect was analyzed in terms of excitatory postsynaptic potential (uEPSP in mV) as well as the increased intracellular dentritic Ca^{2+} concentration, measured by the change of fluorescent intensity (ΔF/F) of the added Ca-ion sensitive dye (Fluo-4, **Figure 5a**). These compared their somatic membrane potential and dendritic Ca^{2+} responses evoked in the presence of **2**–**4** to the ones evoked in the presence of **1**, since the properties of the later compound is being well-documented in the literature.[1,41] The pairwise comparison was performed on the same neuron and same dendritic location.

The same laser intensity, concentration and uncaging time were used during each experiment. All caged materials were bath-applied at a concentration of 2.5 mM. The same laser intensity, which induced only small excitatory postsynaptic potentials (uEPSPs) and small dendritic Ca^{2+} responses (1.43 ± 0.15 mV and 1.22 ± 0.11 ΔF/F, respectively) in the presence of MNI-Glu•TFA (**1**), elicited approximately 10-fold higher responses in the presence of DNI-Glu•TFA (**2**; 15.22 ± 0.28 mV and 7.95 ± 0.25 ΔF/F, respectively, 1st row of **Figure 5b**). The same experiments for DNI-Ulg•TFA (**3**; 2.85 ± 0.29 mV and 1.82 ± 0.12 ΔF/F; 2nd row of **Figure 5b**) resulted significantly less effective results. Interestingly, that MNI-Ulg•TFA (**4**; 0.91 ± 0.18 mV and 0.29 ± 0.10 ΔF/F, 3rd row of **Figure 5b**) proved to be less effective, than the reference compound **1**.

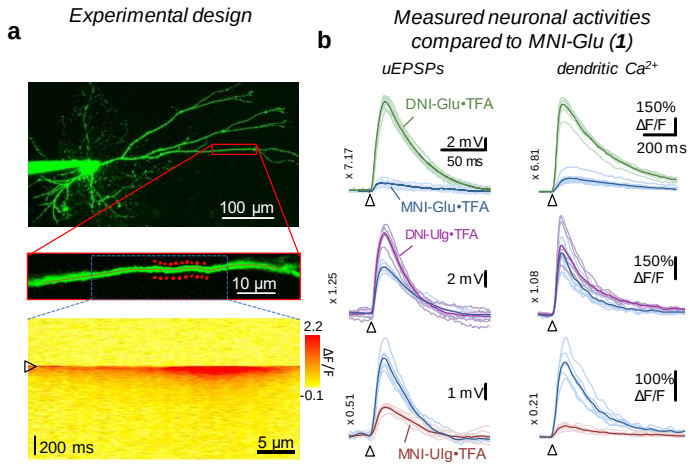

Figure 5*. Comparison of novel caged glutamate compounds **2**–**4** with the reference MNI-Glu•TFA (**1**) in neurophysiological uncaging measurements at constant laser energy (**Method A**). (**a**) (Top) Maximal intensity z projection image of a CA1 interneuron filled with Fluo-4 and Alexa 594. (Middle) Red box shows the enlarged dendritic region of interest. Red points are locations selected for two-photon glutamate uncaging in the presence of DNI-Glu•TFA (**2**, 2.5 mM). (Bottom) Representative uncaging-evoked Ca^{2+} response (average of 5 traces) measured along the red curve in middle. Triangle shows time of uncaging. (**b**) (Left) Two-photon uncaging-evoked somatic excitatory postsynaptic potentials (uEPSPs) in the presence of cage compounds (**1**–**4**). (Right) Simultaneously measured Ca^{2+} transients DNI-Glu•TFA (**2**, green), DNI-Ulg•TFA (**3**, violet), MNI-Ulg•TFA (**4**, red) compared to the responses measured in the presence of MNI-Glu•TFA, (**1**, blue). Bold lines show averages. Triangles indicate uncaging time.*

*1.4.4. Neurobiological comparison experiment at increasing laser intensity of caged compounds **1**–**4** (Method B)*

However, the dendritic and somatic membrane compartments can nonlinearly amplify high-amplitude EPSPs, therefore the overall photochemical yield cannot be determined precisely at a single laser intensity. Thus, we performed a series of uncaging measurements precisely on the same site of the same neuron only for MNI-Glu (**1**) and the most effective DNI-Glu (**2**) (in the sequence of +**1** → wash-in → +**2** → wash-in → +**1**) at increasing laser intensities, as shown in **Figure 6** and **Table 3.** The responses plotted as a function of the second order of the laser intensity and measured the increased photochemical yield as a relative *x*-axis shift of the responses in the presence of DNI-Glu•TFA (**2**) and MNI-Glu•TFA (**1**) by calculating the distance (black arrows) between the two-point sets using unconstrained nonlinear optimization (**Figure 6a,**). The average distance between the two points sets revealed that the release of glutamate with the same rate from MNI-Glu•TFA (**1**) requires 7.17 ± 0.84-fold (ΔF/F) higher two-photon excitation as compared to DNI-Glu•TFA (**2**; $p < 0.00001$, n= 10).

Next (**Figure 6b**), we repeated these experiments by comparing the efficiency of the photochemical release of the reversely coupled compounds, MNI-Ulg•TFA (**3**) and DNI-Ulg•TFA (**4**) relative to the release of MNI-Glu•TFA (**1**). This agreed well with the uncaging experiment, obtained at constant laser energy. The uncaging responses were increased to 5.47 ± 0.49 (p=0.001, n=8) for DNI-Glu•TFA (**2**), and 1.25 ± 0.04 ($p = 0.003$, n = 3) for DNI-Ulg•TFA (**4**) and reduced to 0.51 ± 0.07 ($p < 0.001$, n = 4) in the presence of MNI-Ulg•TFA (**3**) as compared to the reference MNI-Glu•TFA (**1**) (**Figure 6b**, *inset*). Our data showed that the efficiency of photochemical release and the uncaging measurements correlated well for all of the four uncaging materials (R = 0.9877). For details see **[6]**.

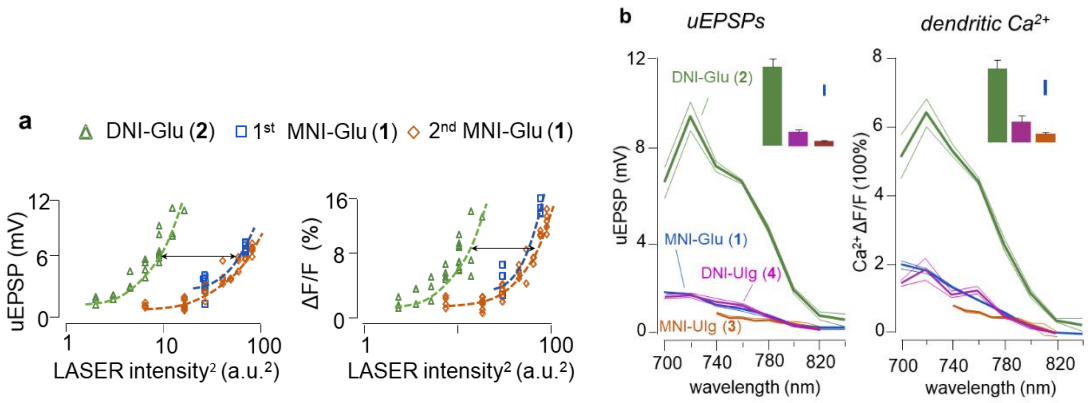

Figure 6. *Comparison of novel caged glutamate compounds in neurophysiological uncaging measurements with varied laser energies (**Method B**). (**a**) Excitatory postsynaptic potential (uEPSP) amplitudes and dendritic Ca^{2+} transient plotted as a function of the second order of the uncaging laser intensity in the presence of MNI-Glu•TFA (**1**, blue squares), following wash-in of DNI-Glu•TFA (**2**, green triangle), and after recovery in MNI-Glu•TFA (**1**, orange diamond). (**b**) Amplitude of uEPSPs (left) and dendritic Ca^{2+} transients (right) evoked in the presence MNI-Glu•TFA (**1**, blue, n=11 neurons;), DNI-Glu•TFA (**2**, green, n=8), DNI-Ulg•TFA (**3**, violet, n=3), MNI-Ulg•TFA (**4**, red, n = 6) as a function of wavelength (mean ± s.e.m). (Inset) The normalized amplitudes of uEPSPs and dendritic Ca^{2+} transients with their errors were measured at 740 nm and normalized to responses of MNI-Glu•TFA (**1**) (blue bars show one unit). In summary, the efficacy of the four compounds studied by different biological methodology (**1**–**4**) are compared in **Table 3**.*

Table 3*. Comparison of the relative efficacy values of MNI-Glu•TFA (**1**), DNI-Glu•TFA (**2**), DNI-Ulg•TFA (**3**) and MNI-Ulg•TFA (**4**), measured in in vitro neurobiological investigations. For details see **Figure 5** and **6**.*

Compounds	**Method A** Rel. to (**1**)	**Method B** Rel to (**1**)
MNI-Glu•TFA (**1**)	1.00	1.00
DNI-Glu•TFA (**2**)	5.47 ± 0.49	7.17 ± 0.84
MNI-Ulg•TFA (**3**)	0.51 ± 0.04	not examined
DNI-Ulg•TFA (**4**)	1.25 ± 0.03	not examined

*1.4.5. Detailed examination of the side-effect of caged compounds MNI-Glu (**1**) and DNI-Glu (**2**) on the GABA receptor*

A further important criterion of a good caged glutamate candidate is the reduced effect on GABA receptor. It was shown earlier that the experimental concentration of MNI-Glu (**1**), like other caged compounds, cause antagonist effect on the GABAergic transmission. Generally, this results in a significant issue, when neuronal circuits are studied, due to the appearance of imbalanced epileptiform events. In addition to that, MNI-Glu typically blocks the GABAergic responses, which prevent the study of inhibitory network activity. Consequently, we measured the effect of DNI-Glu•TFA (**2**) on inhibitory postsynaptic currents (IPSCs) elicited by focal electric stimulation while blocking glutamatergic synaptic transmission (10 µM CNQX and 60 µM AP5) (**Figure 7**). Whereas MNI-Glu•TFA (**1**) in 350 µM reduced the amplitude of IPSCs by 54.3 ± 4.0 % (p = 0.03, n = 5), DNI-Glu•TFA, at the same concentration, did not induce any significant reduction (6.1 ± 5.0 %, p = 0.28, n = 11). These data

undoubtedly show, that the application of DNI-Glu may avoid these side effects, observed during the application of MNI-Glu.

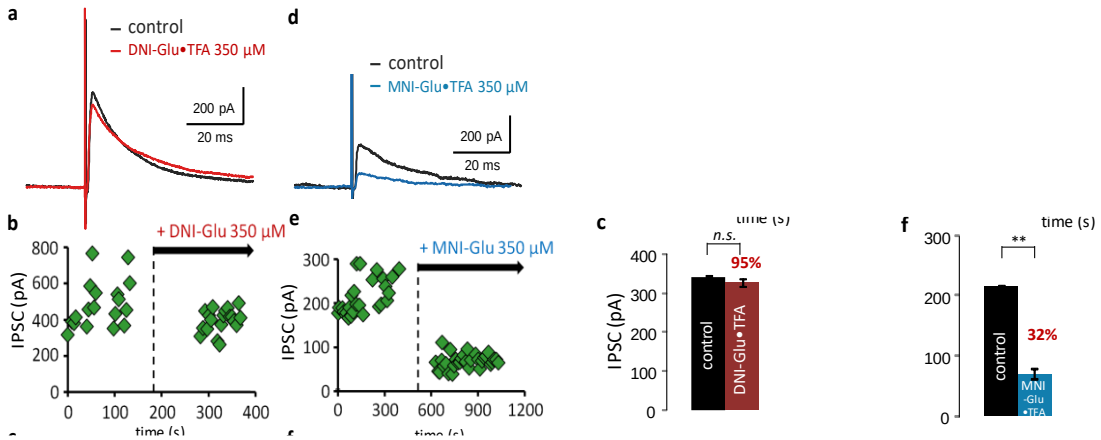

Figure 7*. Effect of DNI-Glu•TFA and MNI-Glu•TFA on IPSCs elicited by synaptic stimulation. (a) Representative IPSCs under control conditions and in the presence of 350 µM DNI-Glu•TFA. Synaptic responses were induced by focal electric stimulation during the blockade of glutamatergic synaptic transmission (10 µM CNQX and 40 µM AP5) in order to isolate GABAergic currents. (b) Amplitude of IPSCs plotted against time. Gray arrow indicates time when DNI-Glu•TFA was added to the bath. (c) Average IPSC amplitudes under control conditions (black) and in the presence of DNI-Glu•TFA. Bars show mean ± s.e.m., n = 5, p = 0.27. (d-f) The same as a-c but for MNI-Glu•TFA. Note the stronger GABA effect of MNI-Glu•TFA. Note also the higher reduction in IPSC amplitude in the presence of MNI-Glu-TFA. Asterisks indicate significance (p < 0.01).*

1.5. Synthesis and development and characterization of novel caged GABA neurotransmitters for three dimensional two-photon uncaging (under publication)

The previous synthetic work was continued to prepare cage-GABA derivatives. Instantly, we have synthetized MNI-GABA (**16**) and DNI-GABA (**17**) according to the earlier synthetic routes, used for Glu derivatives (**Scheme 4**). The yields proved to be attractive (40–60%).

The preliminary biological investigations showed that non-of these compounds exhibit acceptable results, moreover, these compounds proved to rather toxic, than active molecules.

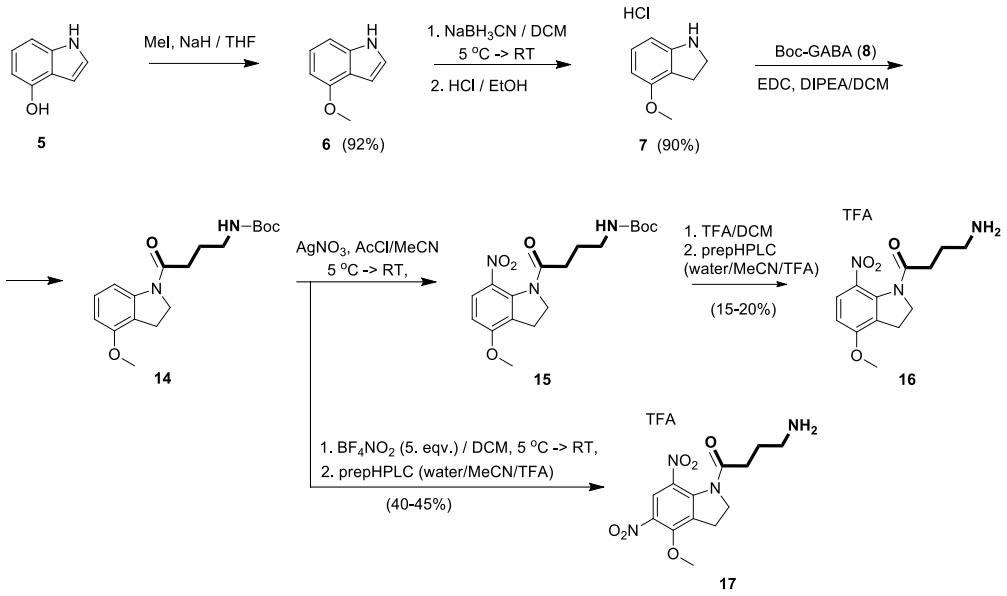

Scheme 4. The synthetic scheme of the trifluoroacetate salts of MNI-GABA (**16**), DNI-GABA (**17**).

We concluded, that the toxicity of MNI-GABA and DNI-GABA can be atributed to their non-expected partial agonism towards GABA receptors, so **16** and **17** trigger the GABA effect immediately. Consequently, we prepared a so called inverse cage-GABA (**21** and **22** on **Scheme 5**) and they were tested. Unfortunately, compounds 21 and 22 did not furnished the desired photo-induced uncaging reaction, so they failed on the test.

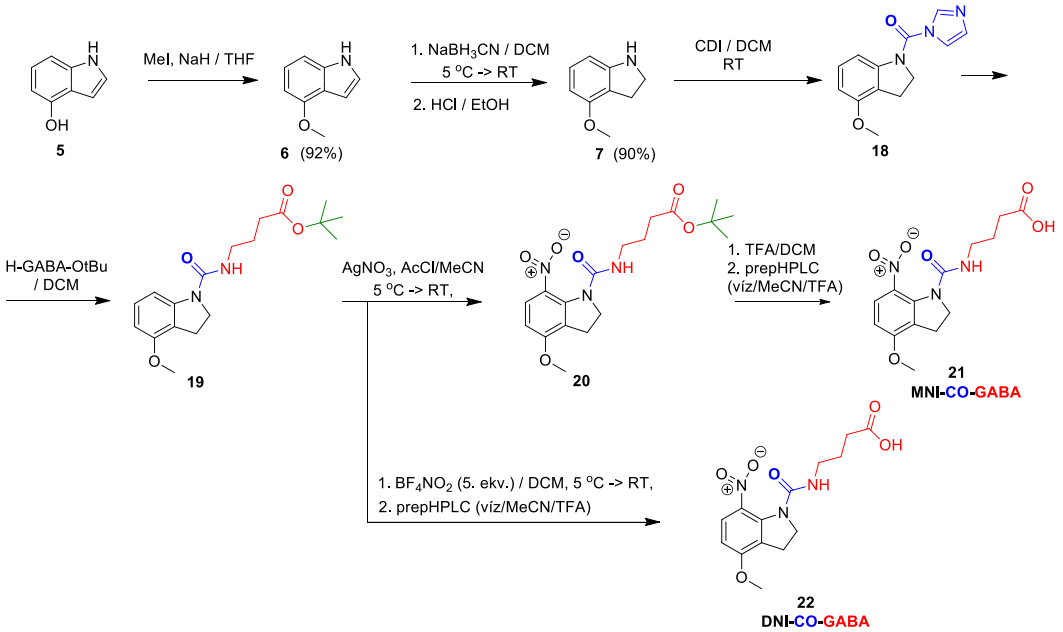

Scheme 5. The synthetic scheme of the trifluoroacetate salts of inverse-MNI-CO-GABA (**21**), inverse-DNI-CO-Glu (**22**).

Paralell to the previous work, we modified the tail of the cage scaffold as shown in **Scheme 6** and **7**. Numerous so called tailed-compounds were prepared accordingly (**27a, b**; **28a,b**; **33a,b** and **34a,b**) developing new synthetic procedure. According the the preliminary biological investigations, they show promishing results, however, this work is on-going presently.

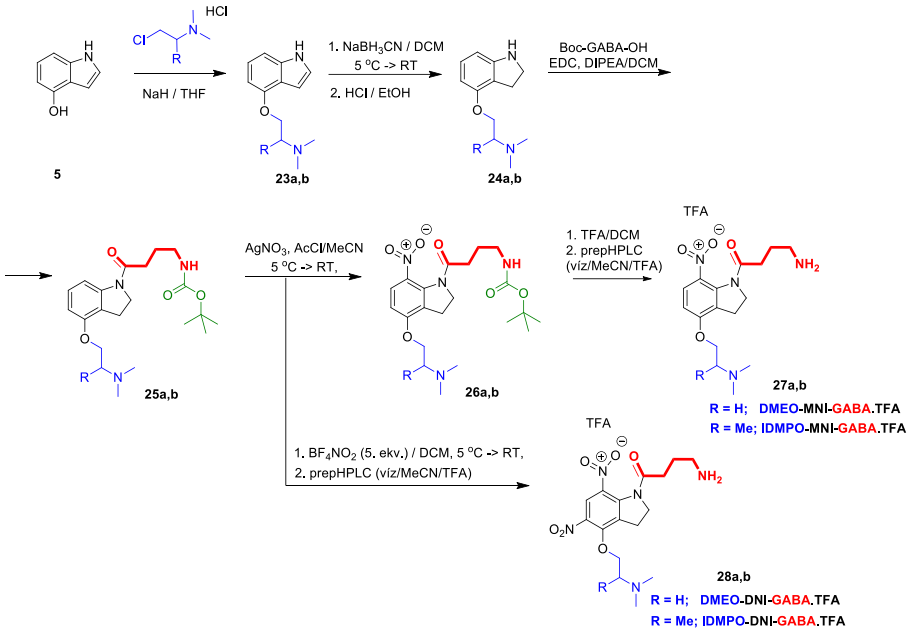

Scheme 6. The synthetic scheme of the trifluoroacetate salts of the tailed-MNI-Glu (**27a,b**), tailed-DNI-Glu (**28a,b**).

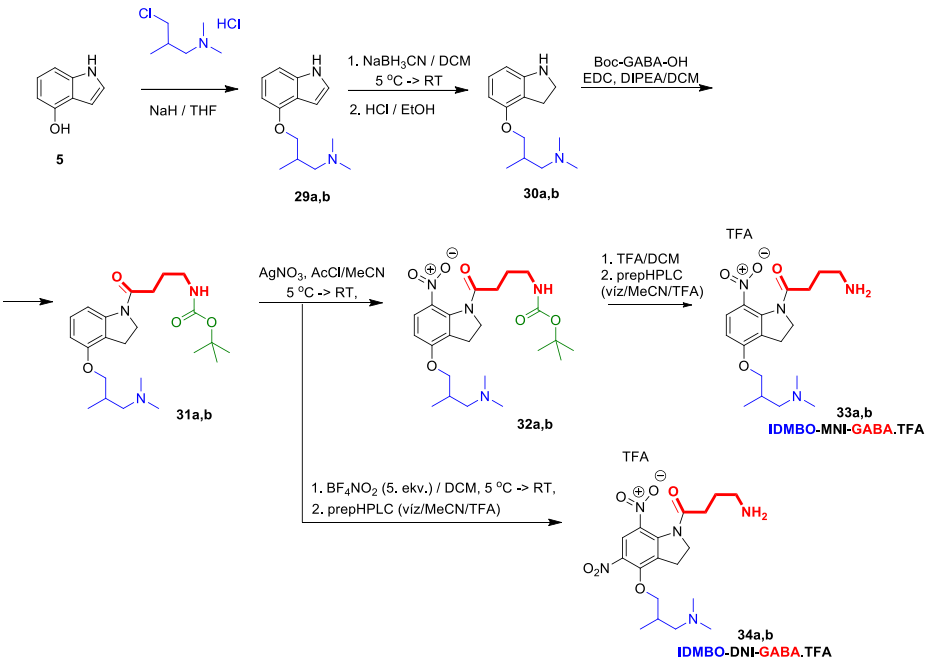

Scheme 7. The synthetic scheme of the trifluoroacetate salts of tailed-MNI-Glu (**33a,b**), tailed-DNI-Glu (**34a,b**),.

Based on the synthetic results and efforts, many other cage compounds were also prepared, and of them (DNI-Gly, DNI-NMDA, DNI-D-Asp) are listed in **Scheme 8**. However, their neurobiological investigations are not lunched.

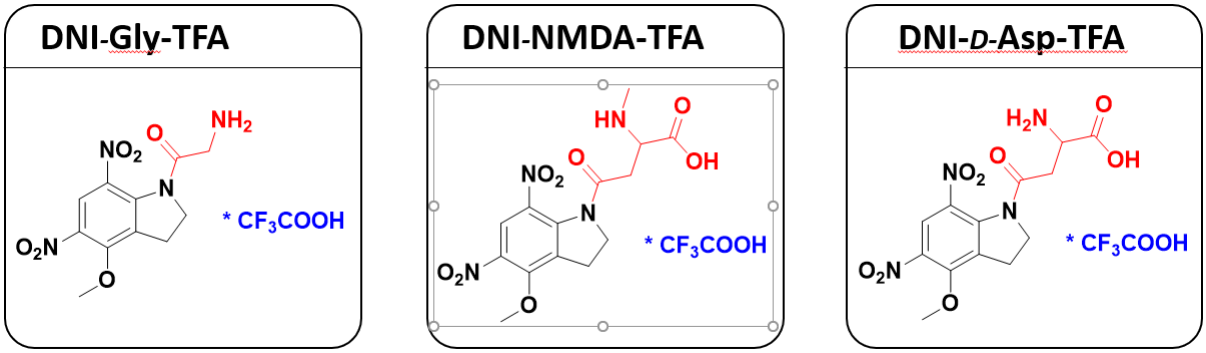

Scheme 8. Other, selected caged neurotransmitters, synthetised during the K_12 grant period.

1.6. References

[1] G. Katona, A. Kaszás, G.F. Turi, N. Hajós, G. Tamas, E.S. Vizi, B. Rozsa Proc. Natl. Acad. Sci. USA **2011**, 108, 2148-2153.
[2] Chiovini, B., Turi, G.F., Katona, G., Kaszas, A., Palfi, D., Maak, P., Szalay, G., Szabo, M.F., Szabo, G., Szadai, Z., Kali Sz., Rozsa B. Neuron **2014**, 82, 908–924.
[3] I. G. Csizmadia, Z. Mucsi, G. Szalay, A. Kaszas, C. H. Lukacsne, O. Majercsik, A. Potor, G. Katona, B. J. Rozsa, D. Gundisch, Dorina; B. Chiovini, D. Palfi, Use of photocleavable compounds U.S. Pat. Appl. Publ. (**2014**), US 20140234883 A1 20140821.
[4] Vasanits-Zsigrai A, Majercsik O, Tóth G, Csámpai A, Haveland-Lukács C, Pálfi D, Szadai Z, Rózsa B, Molnár-Perl I, JOURNAL OF CHROMATOGRAPHY A 1394: pp. 81-88. (**2015**)
[5] Dénes Pálfi, Balázs Chiovini, Gergely Szalay, Attila Kaszás, Gergely Katona, Péter Ábrányi-Balogh, Milán Szőri, Attila Potor, Orsolya Frigyesi, Csilla Lukácsné Haveland, Zoltán Szadai, Miklós Madarász, Anikó Vasanits-Zsigrai, Ibolya Molnár-Perl, Béla Viskolcz, Imre G. Csizmadia, Zoltán Mucsi, Balázs Rózsa; „High efficiency two-photon uncaging coupled by the correction of spontaneous hydrolysis.” Organic & Biomolecular Chemistry **2018**, 16, 1958.

2. Measurement of the membrane potential with silicon carbide nanoparticles

2.1. Objectives, budget and expected results in the research plan

The ultimate goal of the project is to prepare a silicon carbide (SiC) nanosensor of 1-3 nm size that can be excited by two-photon excitation, and the resulting luminescence is sensitive to the presence of Ca ions. These nanosensors can be engineered to the ion channels of the neuron cells, thus the function of brain can be monitored by 3D two-photon microscope developed by the group of Consortium Leader. The report starts with the word-by-word copy of the objectives in the research plan associated with the tasks of Wigner RCP in the collaborative research as written in the beginning of 2012:
"Wigner RCP will apply two basic strategies in order to sharpen the size distribution of silicon carbide nanoparticles (SiC NPs) downto 1-3nm: i) centrifugation of the SiC NP suspension, ii) gel electrophoresis. Our preliminary tests showed that centrifugation of aqueous SiC NP suspension may be used to sort out relatively large (>8nm) SiC NPs. By using high-power centrifugation there is a real hope to filter out even smaller SiC NPs. This needs further investments in Wigner RCP laboratory. In addition, we plan to utilize gel electrophoresis study where the device is already available in Wigner RCP. We will conduct gel electrophoresis with our luminescent SiC NPs where principally one can sort out 1 nm, 2 nm and larger SiC NPs one-by-one by monitoring the emitted light from these nanoparticles. The size distribution will be directly determined by high-resolution transmission electron microscopy. We will use infrared vibration spectroscopy in order to identify the ligands at the surface of SiC NPs. We will quantify the number of ligands by chemical modification of the surface and comparing their corresponding spectra and carry out the treatments in the chemistry lab of Wigner RCP."
This project was planned to be a highly multimodal both in terms in the diversity of applied methodologies – ranging from *ab initio* simulations through sample preparation to sophisticated analysis tools and biological tests – and number of groups in various institutions (IEM HAS, Wigner RCP HAS, Budapest University of Technology and Economics, Roland Eötvös Science University). The budget of the project was planned to mostly spend on chemicals and related materials, user's costs of large equipments (e.g., high resolution transmission electron microscope). In addition, investments were required on small equipments in the beginning of the project that were employed to prepare the samples. Furthermore, part-time work of laboratory assistants (István Balogh and Bence Lázár) was also financed. The costs of participation at international conferences were financed by other sources. 2

2.2. Personnel at Wigner RCP associated with the project

The project started at 2012 with one well-trained PhD student, Dávid Beke. The quality of his work reached rapidly the quality of a well-trained Postdoc (see also Section iv). Later on we involved Gyula Károlyházy in the research as an MSc student who continued with us as a PhD student from 2014. Later on Gabriella Drávecz also worked part-time on this project as a Postdoc researcher from 2015. Regarding the theory side, Bálint Somogyi worked solely on this project as an MSc and later on as a PhD student. Furthermore, Márton Vörös and Viktor Ivády also contributed to this work as a PhD student. In the preparation phase of the semiconductor QDs we part-time employed laboratory assistants (István Balogh, Bence Lázár). In our collaborative research project, many other scientists in Wigner RCP (László Bencs, Károly Lajos Varga, Gábor Bortel, Zsolt Szerkényes, Katalin Kamarás) participated beside the consortium partners in the research, where Zsolt Szekrényes played a crucial role in the analysis of semiconductor nanoparticles. In addition, Zsolt Czigány from the Institute for Technical Physics and Materials Science contributed to this research. We also collaborated with the group of János Erostyák at the University of Pécs from 2014 Summer. We involved a number of students in this research project also as a part of their education. We summarize these efforts in Section iv. In summary, this research project generated cooperation between partners with different expertise that made it truly multidisciplinary.

2.3. Scientific results and their impact at Wigner RCP

In our project, the original research plan focused on three issues: a) produce SiC nanoparticles (NPs) at enhanced yield for biological applications, b) produce 1-3 nm sized SiC nanoparticles that can be engineered into the ion channels of the neuron cells, c) develop protocols to attach Ca sensitive ligand on SiC NPs, in order to make SiC NPs Ca sensitive luminescent nanosensors. Since our SiC NPs have the most intense luminescence in the blue region [1] that is not ideal for *in vivo* imaging we set another target in our research: d) shift the luminescence toward near-infrared (NIR) region.
In the beginning of the project, ***we successfully proved that our SiC NPs can be excited by two-photon excitation in a neuron cell (mouse pyramidal cell), and large concentration of SiC NPs did not alter the biological function of the cell for long time.*** This experiment supported our vision that SiC NPs can be a stable and biocompatible nanomarker to monitor neural activities. This result was published in the *Journal of Materials Research* [2]. The luminescence could be detected mostly in the red region where the intensity of SiC NPs' luminescence is much smaller than that in the blue region. We concluded that the absorption of the cell and the autofluorescence hid the signal of SiC NPs at the blue region, so we parallel started to work to produce such luminescence centers inside SiC lattice that may shift the luminescence toward red. *Ab initio* calculations implied [3,4] that this can be achieved either by metallic dopants or donor-acceptor pair doping, or vacancy-related point defects. We carried out different theoretical and experimental studies to investigate this issue in international collaboration [5–9] that was published in two *Nature Materials*, one *Nature Communications*, and one *ACS Nano* and one *Talanta* papers. Here, we were able to identify carbon-antisite vacancy defect as a bright red emitter, a combination of Si-antisite defect in polytype inclusion of SiC as bright visible emitter. So far, we were able to introduce these defects into larger SiC nanoparticles with relatively low yield [6]. We are still working to increase the yield of bright red or NIR emitters in small SiC NPs. (**Figure 8**)

We solved the issue to produce SiC NPs at large yield. We developed the synthesis of SiC ceramic powder and the stain etching method we use for SiC NPs synthesis from SiC powder. In the original method the mixture of SiC powder, HF and HNO_3 was heated up in an open system like in a round flask made from fluorinated polymer. These limit the maximum temperature that can be reached because of the boiling point of the mixture (which is about 110°C) based on the boiling point of hydrofluoric acid (108°C) and nitric acid (122°C). It is also worth to mention that despite careful construction of the reactor, the release of such toxic and corrosive vapors to the fume hood cannot be eliminated completely. Therefore, we transferred these reactions to a closed acid digestion system that can be heated up to 250°C and acids contact with the environment only at ambient temperature and for a limited time. Both the optimal temperature and reaction time were determined. We found that 2 hours annealing time and 150°C annealing temperature give the best results. This development led to the reduction the size distribution from 1-16 nm down to 1-8 nm and the increase the yield of the NPs from 2 mg to 3.5 mg by etching 2.5 g SiC.
The NPs yield depends on the volume of porous layer formed during the etching. We found that increasing the time do not increase the volume of porous layer therefore we increased the surface area by developing new synthesis route for SiC powders. The SiC was firstly prepared as follows: Silicon and graphite powder were mixed with a molar ratio of 1:1.2 in an alumina mortal and pressed into a pellet, then placed into an induction chamber and heated under argon to about 1300 °C where the reaction began. In these cases, heating is possible due to the conductivity of graphite. When Si and C reacted to form SiC, pellet lost its conductivity and the heating stopped. According to scanning electron microscope images, micron size SiC grains formed with low porosity. SiC produced with combustion synthesis method usually conserve the morphology of the graphite source. Therefore, activated charcoal with high surface area was chosen. Because the mixture of charcoal and Si powder cannot be pressed into a pellet, the resistivity of such samples stemmed the direct annealing in an induction furnace. We redesigned the furnace for our new samples. In the new system, the mixture is annealed in a graphite crucible that we also designed for this purpose. By using Si powder and charcoal as a carbon source and a small amount of polytetrafluoroethylene (PTFE) that propagates the reactions, we are able to produce cubic SiC powder with very high surface area.

By using the new SiC source we were able to prepare 65 mg SiC NPs from 2.5 g SiC. This corresponds to 20 times enhancement in the yield. Furthermore, we scaled up the stain etching by installing 250 ml acid digestion vessel in lieu of the 23 ml vessels. The maximum operating capacity is about 4600 mg SiC NPs in a week which makes possible to produce SiC NP samples for functionalization to our partners at IEM HAS. The development of producing SiC NPs was published in a *Journal of Materials Research* paper [10].

We produced 1-3 nm SiC NPs with using special filters and dialysis technique. We could separate this fraction from a larger fraction with a size of > 6 nm. Surprisingly, the molecular-size fraction did not show quantum confinement related luminescence at all whereas the fraction of large particles exhibited a weak, band edge or stacking fault related luminescence. This result was published in *Nanoscale* journal [11]. Later, we proved by time-dependent photoluminescence (PL) studies that the luminescence of molecular-sized SiC NPs originate from carbon-oxygen surface groups and an emitter residing at the thin oxide layer on SiC NPs (published in *The Journal of Physical Chemistry C* [12]). In summary, we could achieve a milestone in the research by producing 1-3 nm SiC NPs. However, the origin of the emitter revealed that further separation of this ultrasmall SiC NPs has no real advantage in the nanosensor application, thus we rather focused our studies on the functionalization of these SiC NPs. 4

We proved that a Ca sensitive dye was attached to SiC NPs that turned the luminescence of molecular-sized SiC NPs sensitive to the presence of (Ca) ions. Here we reached two milestones to achieve this result. First, we carried out a temperature dependent infrared and photoluminescence spectroscopy study, combined with *ab initio* modeling, in order to reveal the chemical transformations of the surface termination groups of SiC NPs in aqueous solution. We found that at temperatures above 370K, acid anhydride groups form by condensation of water between neighboring carboxyl groups. The presence of the anhydride groups revealed the proximity of the carboxyl groups and represented a new possibility of selective engineering of new hybrid materials involving SiC NPs. The latter can be achieved by the very reactive anhydride groups that can be used to attach many types of molecules for functionalization. The results were published in *The Journal of the Physical Chemistry C* [13]. Second, we were able to develop methods for quantitative determination of technically important surface groups. By using potentiometric titration [12] we could determine the concentration of dissociative groups. Indeed we found that three types of dissociation occur in a SiC aqueous colloid that is in agreement with infrared absorption studies that had showed three groups that have acid-base characteristic, namely, carboxyl groups (COOH), hydroxyl groups (C-OH) and silanol groups (Si-OH). Combining gravimetric analysis with size distribution and titrimetric measurements we determined the number of these groups on the surface of SiC NPs. An average 3 nm SiC NPs is covered by ≈100 carboxyl moieties, ≈30 C-OH and ≈10 Si-OH groups.

By combining these two results above we could calculate the concentration of carboxyl groups in the colloid solution that could be transformed to reactive anhydride groups. This was the base to design a protocol to attach a Ca sensitive dye to the molecular-sized SiC NPs as follows.

Most of the currently used Ca sensitive dyes are 1,2-bis(o-aminophenoxy)ethane-N,N,N′,N′-tetraacetic acid (BAPTA) derivatives. Our idea was to attach BAPTA to SiC NPs' surface, in order to turn SiC NPs Ca sensitive. We used amine functionalized BAPTA with methyl ester protecting group for attaching to the SiC surface. First, we produced anhydride groups on SiC surface. We thought that amino-BAPTA can react with anhydride groups to form peptide bonds, therefore, it would covalently attach to the SiC surface. The reaction would have no byproducts. We estimated the concentration of anhydride groups on SiC surface. In order to prove this protocol, we added amino-BAPTA molecules to SiC NPs with anhydride groups, in collaboration between Wigner RCP and IEM HAS research groups. After surface termination the methyl ester protecting group was hydrolyzed, in order to activate the Ca sensitivity of BAPTA (see Fig. 1).

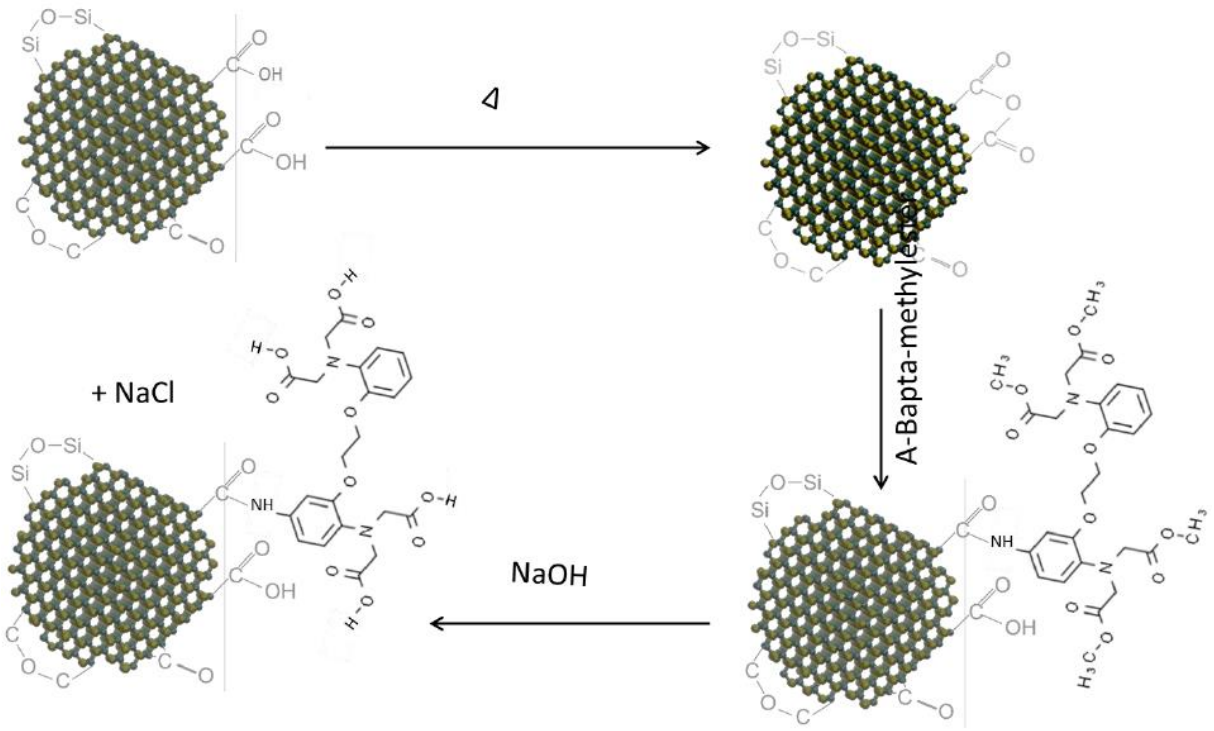

***Figure 8**. The reaction mechanism*

We note here that surface termination of nanoparticles has several challenges. For example, the molecule expected to form covalent bonds on the surface of SiC NPs can also interact with these nanoparticles through physisorption. To avoid unwanted mechanism, we setup a characterization protocol to follow the reaction with infrared absorption spectroscopy (FTIR):

1. The characteristic IR spectrum of BAPTA molecule differ from that of SiC NPs that makes FTIR measurements suitable for following the reaction, however, the contrast in the IR vibration spectrum of amide bonds and carboxyl bonds is small that makes challenging to determine the successful covalent bond formation.

2. Furthermore, the hydrolyzation process should be also followed in the FTIR spectrum. In other words, the ester vibrations and acid vibrations should be distinguished but the IR spectra of SiC and BAPTA can overlap with the vibration of these groups.

To overcome this problem, we developed a very effective separation procedure based on ion exchange resins that can remove unreacted BAPTA from SiC colloid solution. Therefore, only the covalently attached BAPTA molecules contribute to the signal in the IR spectrum. Next, we followed the hydrolysis with FTIR from the start to the total hydrolysis where the peptide bond was hydrolyzed too (see **Fig. 9**).

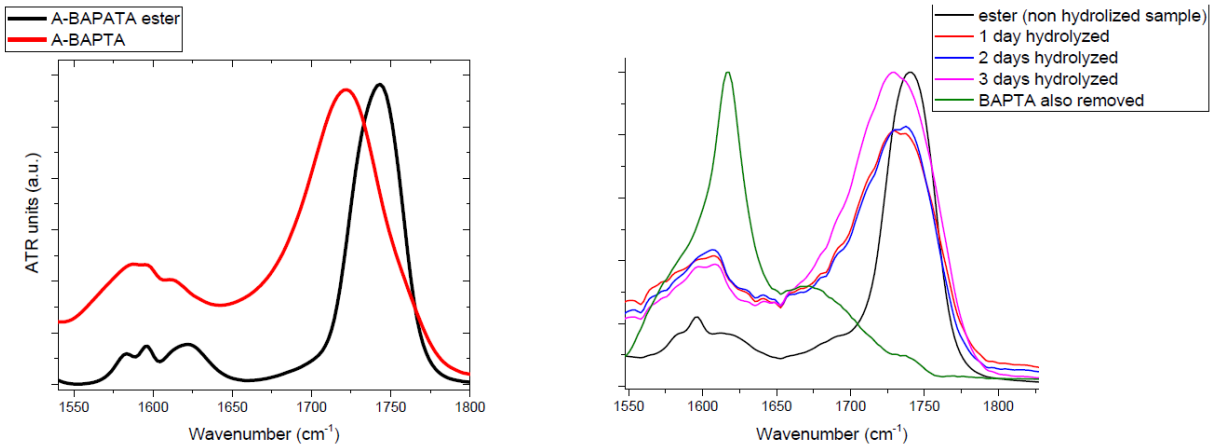

***Figure 9**. FTIR spectra of BAPTA molecules under various conditions*

As can be seen in Fig. 2, the peak of ester appears at higher wavenumbers (1750 1/cm) than that of the corresponding carboxylic acid (1680 1/cm). Even tough, the IR spectrum of carboxyl moieties on the SiC surface interfere with that of carboxyl acid groups of BAPTA, by following the hydrolysis we determined reference points in the IR spectra that can be used to determine the stage of hydrolysis. These results imply that we could successfully bond BAPTA molecules to SiC NPs with covalent bonds that we label by SiC@BAPTA.

We characterized the PL spectrum of SiC@BAPTA system by varying the numbers of BAPTA molecules on the SiC surface at different pH levels. Even when a single BAPTA molecule is attached to SiC NPs the peak of SiC NPs at 450 nm shifts to 390 nm in the composed system (see **Fig. 10**). The full PL spectrum of SiC@BAPTA is similarly broad as that of SiC NPs. When many BAPTA molecules are attached to SiC NPs then the emission has the maximum intensity at 470 nm (see **Fig. 10**). By studying the excitation dependence of these two peaks we found that the two peaks had maximal emission intensity at different excitation energies (see **Fig. 11**). We concluded that these peaks originate from independent emissions. Further studies are needed to reveal the origin of these emissions.

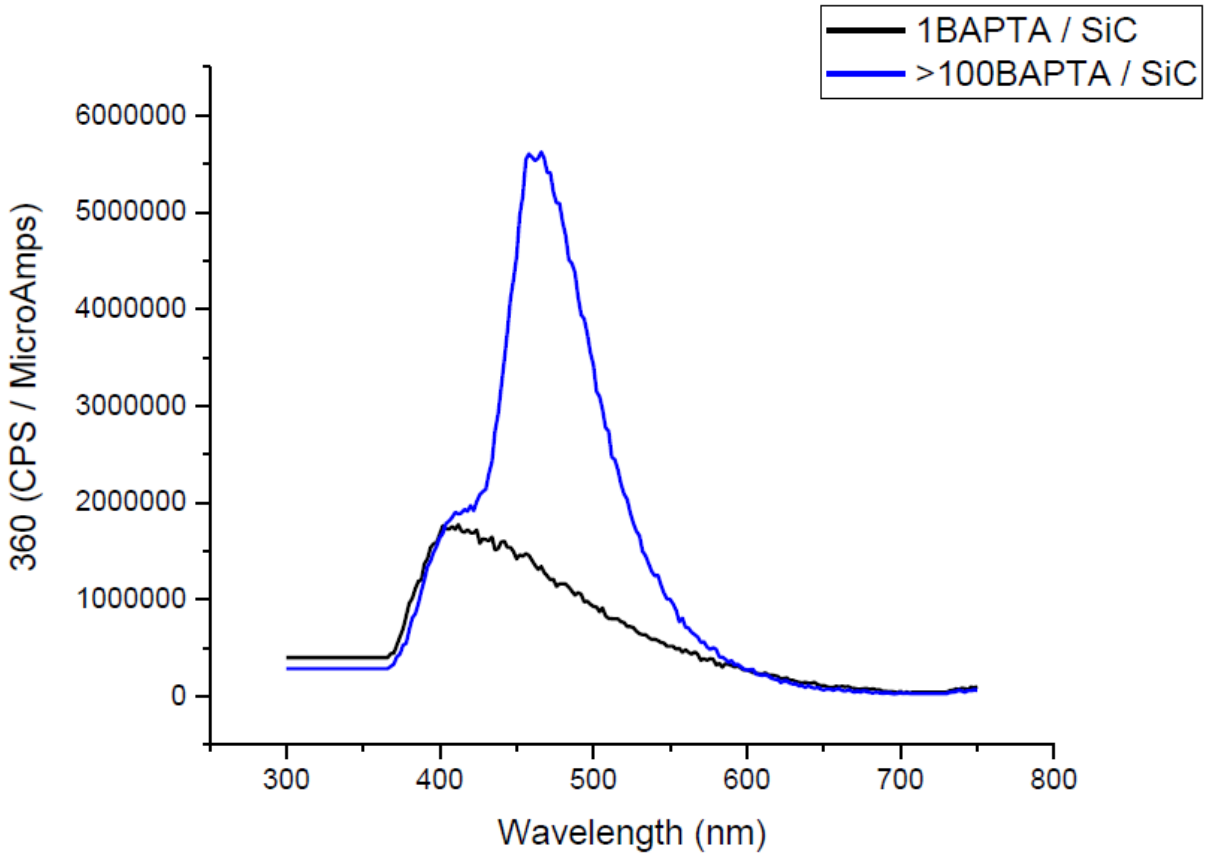

Figure 10*. Photoluminescence spectra of SiC NPs attached to a single BAPTA molecule (black curve), or with total coverage of BAPTA molecules (blue curve).* 7

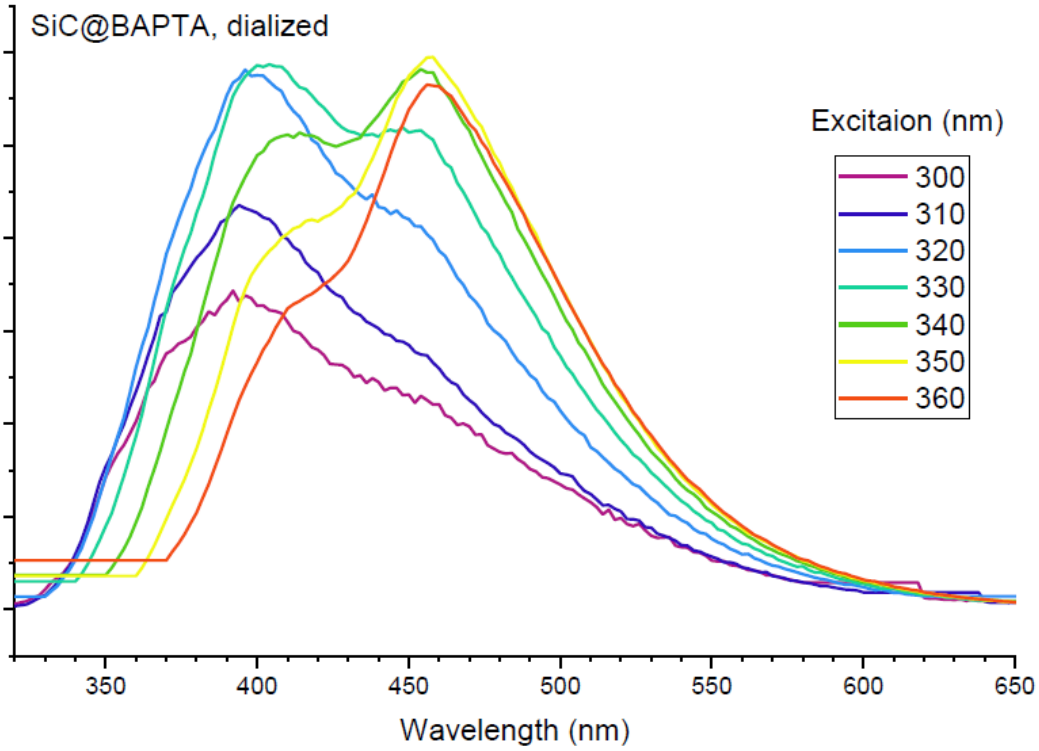

Figure 11. *Excitation energy dependence of the photoluminescence spectrum of SiC@BAPTA*

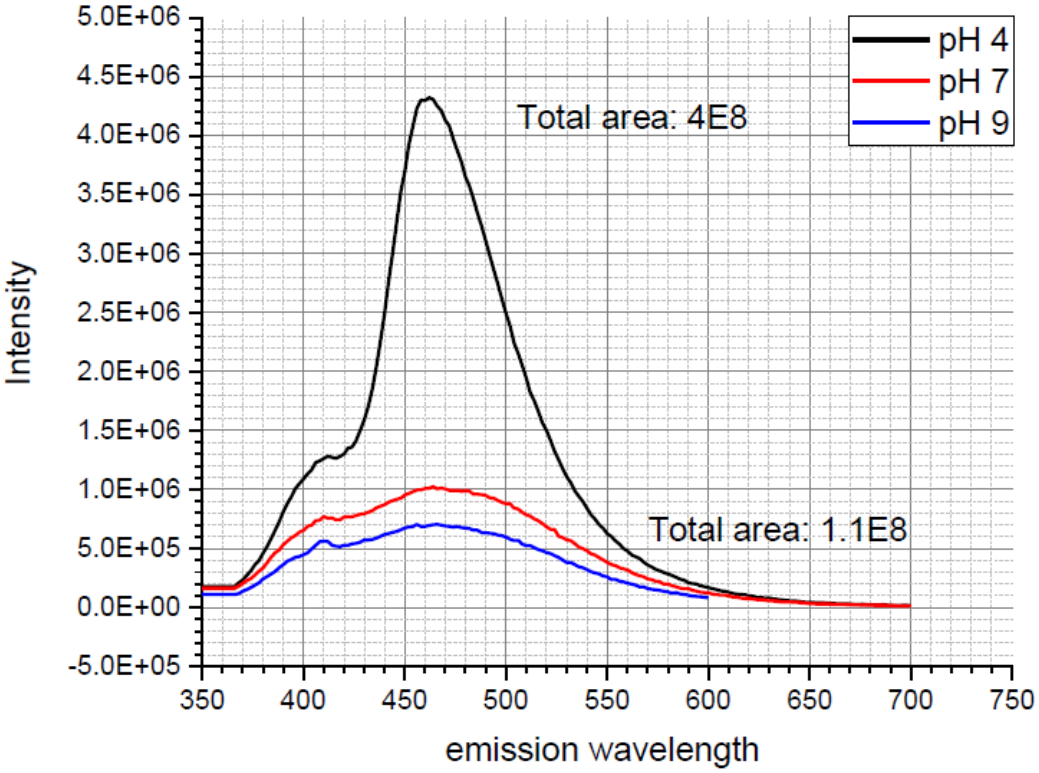

Figure 12. *Photoluminescence spectrum of SiC@BAPTA as a function of pH value* 8

At this stage of the research we have been unable to measure directly the optical respond of SiC@BAPTA to Ca concentration because solvent exchanges and hydrolysis increased the salt concentration in SiC@BAPTA colloid solution, and the concentration of ions were too high to measure the Ca sensitivity of SiC@BAPTA system in such solution. On the other hand, we could measure the pH sensitivity of their PL signal that should reflect the response of SiC@BAPTA to environmental changes. Indeed, below the pKa value of carboxyl acid the overall intensity of emission increased about five times with respect to the solution at higher pH values (see Fig. 5). This clearly proves that SiC@BAPTA system acts as a nanosensor.
The results on SiC@BAPTA system are unpublished. We are still working to show the contrast and/or shift in the PL spectrum of SiC@BAPTA system as a function of Ca concentration in the region which is typical in the neuron cells. When this sensitivity is determined then we will test this system by our 3D two-photon microscope *in vivo*. The successful measurements would represent a breakthrough in the field.

Finally, ***we could amine-terminate our SiC NPs.*** We successfully applied different reduction reactions on SiC NPs [12] that can produce fully hydroxyl or fully silanol terminated SiC NPs. Hydroxyl and silanol terminated SiC NPs can be easily modified with silane coupling agents. We attached 3-aminopropyldimethylethoxysilane to the surface of SiC NPs that produced amine-terminated SiC NPs. This can be a route to introduce our SiC NPs into the ion channels of neuron cells.
In summary, we could achieve the objectives associated with Wigner RCP in the research consortium. We developed methods to produce SiC NPs at enhanced yield, we produced 1-3 nm molecular-sized SiC NPs, we attached BAPTA molecule to SiC NPs in a controlled fashion and developed methods to change the polar groups to apolar groups at the surface of SiC NPs. We published ten papers about these results mostly in D1 or Q1 journals. We are testing now our developed SiC@BAPTA system that is a promising Ca nanosensor for *in vivo* detection of neuron activity.

2.4. References

[1] D. Beke, Z. Szekrényes, I. Balogh, M. Veres, É. Fazakas, L. K. Varga, K. Kamarás, Z. Czigány, and A. Gali, Appl. Phys. Lett. **99**, 213108 (2011).
[2] D. Beke, Z. Szekrényes, D. Pálfi, G. Róna, I. Balogh, P. A. Maák, G. Katona, Z. Czigány, K. Kamarás, B. Rózsa, L. Buday, B. Vértessy, and A. Gali, J. Mater. Res. **28**, 205 (2013).
[3] B. Somogyi, V. Zólyomi, and A. Gali, Nanoscale **4**, 7720 (2012).
[4] B. Somogyi and A. Gali, J. Phys. Condens. Matter **26**, 143202 (2014).
[5] S. Castelletto, B. C. Johnson, V. Ivády, N. Stavrias, T. Umeda, A. Gali, and T. Ohshima, Nat. Mater. **13**, 151 (2014).
[6] S. Castelletto, B. C. Johnson, C. Zachreson, D. Beke, I. Balogh, T. Ohshima, I. Aharonovich, and A. Gali, ACS Nano **8**, 7938 (2014).
[7] M. Widmann, S.-Y. Lee, T. Rendler, N. T. Son, H. Fedder, S. Paik, L.-P. Yang, N. Zhao, S. Yang, I. Booker, A. Denisenko, M. Jamali, S. A. Momenzadeh, I. Gerhardt, T. Ohshima, A. Gali, E. Janzén, and J. Wrachtrup, Nat. Mater. **14**, 164 (2015).
[8] A. Lohrmann, N. Iwamoto, Z. Bodrog, S. Castelletto, T. Ohshima, T. J. Karle, A. Gali, S. Prawer, J. C. McCallum, and B. C. Johnson, Nat. Commun. **6**, 7783 (2015).
[9] G. Dravecz, L. Bencs, D. Beke, and A. Gali, Talanta **147**, 271 (2016).
[10] D. Beke, Z. Szekrényes, I. Balogh, Z. Czigány, K. Kamarás, and A. Gali, J. Mater. Res. **28**, 44 (2013).
[11] D. Beke, Z. Szekrényes, Z. Czigány, K. Kamarás, and Á. Gali, Nanoscale **7**, 10982 (2015). 9
[12] D. Beke, T. Z. Jánosi, B. Somogyi, D. Á. Major, Z. Szekrényes, J. Erostyák, K. Kamarás, and A. Gali, J. Phys. Chem. C **120**, 685 (2016).
[13] Z. Szekrényes, B. Somogyi, D. Beke, G. Károlyházy, I. Balogh, K. Kamarás, and A. Gali, J. Phys. Chem. C **118**, 19995 (2014).

2.5. Contribution to education and involvement of students in the research

Students were involved in the research of this project at various grades. **Dávid Beke**'s doctoral thesis entitled "Fabrication and characterization of silicon carbide nanoclusters" is partially based on the achieved results in the project. He plans to defend his thesis this year as he already passed the doctoral examination. ***Dávid Beke is a key researcher in the experimental group working at the level of a well-trained Postdoc researcher.*** He presented the results at various conferences where he received great attention. Particularly, I underline the Graduate Student Award at EMRS symposium that was given to award his talk entitled "Identification of Luminescence Centers in Molecular-Sized Silicon Carbide Nanocrystals" on the latest results achieved on characterization of SiC nanoparticles.
Zsolt Szekrényes participated in the research as a PhD student from Prof. Katalin Kamarás group and two thesis points of his thesis entitled "Study of complex nanostructures by infrared spectroscopy" are based on the results obtained in the project. Zsolt Szekrényes successfully graduated in 2015 as a physicist. Later on **Gyula Károlyházy** joint our research as an undergraduate student and he received his MSc as chemical engineer at the Budapest University of Technology and Economics with the diploma entitled "Fémmel adalékolt SiC nanokristályok előállítása és vizsgálata (Preparation and characterization of silicon carbide nanocrystals doped by metal elements)" in 2014. He is now a PhD student in the group working solely on the project as youth researcher at Wigner RCP. He plans to start the doctoral degree process by the beginning of next year where his doctoral thesis points will be partially based on the results achieved in the project. On the theory side of the project **Bálint Somogyi** obtained important results. He received his MSc degree in physics in 2012 entitled "Félvezető biomarkerek vizsgálata első elvű számításokkal (Study of semiconductor biomarkers by *ab initio* calculations)" and he continued as a PhD student at the Doctoral School of Physics at the Budapest University of Technology and Economics working entirely on this project. He already started the doctoral degree process and plans to defend his thesis entitled "Semiconductor biomarkers for biological imaging: A first principles study" in early 2017. He received "Publication Award" at the Department of Atomic Physics of the Budapest University of Technology and Economics in 2012 and 2014. He got a pledge at the OTDK (National competition on scientific achievements by undergraduate students) in 2013. **Viktor Ivády** contributed to identification of important color centers in SiC and understanding the properties of metal impurities in SiC that were of high importance in the project. He started his PhD in 2011 and he will defend his thesis entitled "Development of theoretical approaches for post silicon information processing" on November 11, 2016. One of his thesis points is particularly associated with the project on identification of single photon sources in SiC. Finally, **Tibor Zoltán Jánosi** from János Erostyák group defended his PhD thesis entitled "Fluoreszcens módszerek alkalmazása nanostruktúrák vizsgálatában (Study of nanostructures by means of fluorescence methods)" in 2016 where two thesis points are based on the results obtained in the project.
We involved many young students from the Faculty of Chemical Technology and Biotechnology of the Budapest University of Technology. As our project planned to employ our nanoparticles in biological systems we could attract these students from the fields of materials science and biochemistry. The 10 students often participated in the research as a part of their regular education at the University in the frame of practices either during the semester ("Önálló feladat") or summer time ("Nyári gyakorlat"). Some of the students obtained BSc degree in these activities or they plan to submit their BSc work or MSc work in the next year. Beside their regular activities they came to our laboratory to carry out research in their free time, and they participated in the competition on scientific achievements by undergraduate students (TDK) at the University, or they plan to submit their work this year. In terms of numbers, two BSc and two MSc degrees were partially based on the results of this project. Besides three (O)TDK works summarized the results of the project. Furthermore, two PhD degrees relied on the results associated with the project, and three other PhD theses will be soon finished that use the results of the project. In addition, three MSc and one BSc works as well as two TDK works will be submitted this year or next year that are partially associated with the results of the project.

2.6. Outreach of the project

Beside the rise of a new "school" on preparation of semiconductor nanoparticles at Wigner RCP, the PI has reorganized and developed the laboratories that contribute to the fabrication of samples and their manipulation by chemistry, annealing, and so on. The PI founded the Wigner Advanced Materials Integrated Laboratory (Wigner ADMIL) that was supported by infrastructural grant of the Hungarian Academy of Sciences in 2015 and was registered in the list of national scientific infrastructures [http://wigner.mta.hu/admil/]. The scientific work and achievements in this project contributed to the foundation of this open-access laboratory.